



# Fluorescent and thermoresponsive tetraphenylethene-based cross-linked poly(*N*-isopropylacrylamide)s: Synthesis, thermal/AIE properties, and cell viability

Meng-Tzu Weng<sup>a,b</sup>, Amal Farghal Noreldein Elsyed<sup>c</sup>, Po-Chih Yang<sup>c,\*</sup>,  
Mohamed Gamal Mohamed<sup>d,e</sup>, Shiao-Wei Kuo<sup>d</sup>, Kuen-Song Lin<sup>c,\*</sup>

<sup>a</sup> Department of Internal Medicine, National Taiwan University Hospital, Taipei City 100233, Taiwan

<sup>b</sup> School of Medicine, College of Medicine, National Taiwan University, Taipei, Taiwan

<sup>c</sup> Department of Chemical Engineering and Materials Science, Yuan Ze University, 135, Yuandong Rd, Chung-Li District, Taoyuan City 32003, Taiwan

<sup>d</sup> Department of Materials and Optoelectronic Science, Center of Crystal Research, National Sun Yat-sen University, Kaohsiung City 80424, Taiwan

<sup>e</sup> Chemistry Department, Faculty of Science, Assiut University, Assiut 71516, Egypt

## ARTICLE INFO

### Article History:

Received 18 October 2021

Revised 12 January 2022

Accepted 25 January 2022

Available online 5 February 2022

### Keywords:

Drug delivery

Cell tracking

Tetraphenylethene

PNIPAm

RAFT

## ABSTRACT

**Background:** The synthesis, thermal properties, and aggregation-induced emission (AIE)-responsive properties of a series of tetraphenylethene (TPE)-based cross-linked poly(*N*-isopropylacrylamide)s (PNIPAm)s consisting of a hydrophilic/thermosensitive NIPAm monomer and AIE-responsive/hydrophobic TPE derivative through reversible addition-fragmentation chain transfer polymerization was investigated in this study.

**Methods:** The AIE effect was investigated in a H<sub>2</sub>O/THF mixture via photoluminescence intensity measurements, and the polymers showed emission ( $\lambda_{em} = 485 \pm 5$  nm). When the water fraction was 90%, the PL intensity was enhanced to the highest value.

**Significant findings:** Polymers P1–P3 showed the low critical solution temperature (LCST) at approximately 33.5, 32.4, and 28.1 °C, respectively, and deformed at P4 and P5. From dynamic light scattering, the hydrodynamic diameters of P0 and P1–P2 at a temperature higher than the LCST decreased from 564.0 to 159.6 nm, 417.4 to 126.7 nm, and 469.4 to 134.5 nm (P0, P1, and P2, respectively), indicating the thermoresponsive property. A MTT assay was used for HepG2 liver cancer cells at a concentration of 2  $\mu$ g/mL, and all the polymers showed cell viability over 80%. P2 and P3 showed emission in the living HepG2 cells for 96 h of incubation. These findings suggest that the synthesized polymers have potential as drug carriers.

© 2022 Taiwan Institute of Chemical Engineers. Published by Elsevier B.V. All rights reserved.

## 1. Introduction

Liver cancer is one of the most widespread cancers, and in 2018, it was identified as the sixth most common cancer and the fourth leading cause of cancer deaths worldwide. Various cancer treatments are used worldwide, such as surgical resection, transplantation, ablation, embolization, radiotherapy, targeted therapy, chemotherapy, and immunotherapy. Chemotherapy remains the main method of treatment for patients with cancer; however, this treatment lacks selectivity and induces damage to normal cells [1–3]. Targeted drug delivery is a promising method for overcoming the obstacles of conventional cancer treatments. Nanotechnology is applied in cell imaging, cell tracking, and targeted therapy and provides a more effective treatment with fewer side effects. It also enables tracing of drug accumulation and metabolism in cells [4]. Self-assembly polymeric micelles

(PMs) are versatile carriers for drug delivery and nucleic acids as they have favorable physicochemical properties, such as biocompatibility, bioavailability, circulation time, drug loading, and controlled release abilities. Additionally, the presence of the hydrophobic core makes PMs a good choice for overcoming the problem of the short circulation time and systemic toxicity in water-insoluble chemotherapeutic agents [5–8]. Recently, many PMs based on the hydrophilic/thermosensitive NIPAm monomer (PM shell) and aggregation-induced emission (AIE)-responsive/hydrophobic tetraphenylethene (TPE; PM core) [9–12] have been utilized to derive conjugated polymers with both emission and temperature sensitivity. Thus, PMs are good candidates for controlled/targeted drug delivery as well as cell imaging and tracking.

Poly(*N*-isopropylacrylamide) (PNIPAm) is a thermo-responsive switchable polymer that can switch between the water-soluble and insoluble state in response to temperature changes [13]. These reversible phenomena occur hundreds of times upon heating and cooling without affecting or destroying the polymer chain. The low

\* Corresponding authors.

E-mail addresses: [pcyang@saturn.yzu.edu.tw](mailto:pcyang@saturn.yzu.edu.tw) (P.-C. Yang), [kslin@saturn.yzu.edu.tw](mailto:kslin@saturn.yzu.edu.tw) (K.-S. Lin).

critical solution temperature (LCST) of PNIPAm (32.0 °C in water) makes it suitable for various applications, especially biomedical applications (controlled drug delivery, self-healing materials, tissue engineering, regenerative medicine, etc.) [14–17]. The LCST of PNIPAm-containing polymers depends on the polymer compositions and many other factors, such as the type of comonomers (hydrophilic or hydrophobic), molecular weight, chemical nature of the chain end, multi-solvent systems, salts, critical gel concentration, and end-group or terminal unit of side chain [18,19]. PNIPAm-containing fluorophores have been applied and investigated in several studies. Kim et al. [20] demonstrated that the hydrophobic field near the fluorophore unit increased upon increasing the temperature and the fluorescence intensity of P(NIPAm-co-SPO-co-fluorophore) also enhanced. Moreover, Li et al. [11] proved that the intrachain or inter-chain hydrogen bonds within oligo(ethylene glycol) methacrylate-based PNIPAm form fluorescent aggregates at a temperature higher than the LCST.

Aromatic and classical luminophores emit strongly in their spread states or dilute solutions. When they are aggregated or clustered, they undergo various degrees of light emission quenching, which is known as the aggregation-caused quenching (ACQ) effect. Thus, the ACQ effect limits the application of these conventional fluorescence materials in the aggregated or solid state [21,22]. In contrast, AIE luminogens (e.g., TPE) emit strongly in the aggregate or solid state and demonstrate weak or faint emission in the molecularly dispersed state or dilute solutions [23–32]. The AIE phenomenon was first demonstrated by Tang et al. in 2001 [33]. Photophysical properties of the fluorescent materials are influenced by their molecular structures, conformations, and morphological arrangements [34]. Restriction of intramolecular motions is the main reason for the AIE effect as it causes radiative decay of excitations. In addition, the propeller shape reduces the stacking interactions between the molecules, thus, the ACQ phenomenon does not occur or is limited [35–38]. The unique behaviors of AIE luminogens make them the focus of studies, and several types of AIE have been designed and incorporated in different fluorescent systems for several applications (e.g., bioimaging, optoelectronics, chemosensing, stimuli-responsive systems) [21,39]. Su et al. [40] reported that a fluorescent benzoxazine derivative (TPE-BOZ) was used as an optical probe to determine the presence of picric acid, and TPE-BOZ showed the AIE property in a mixture of ethanol/H<sub>2</sub>O. Li et al. [41] synthesized an organic–inorganic thermoresponsive polymer (POSS-*b*-PNIPAM) encapsulating TPE and investigated the effect of temperature on the photoluminescence (PL) intensity of TPE. They found that when the temperature was close to the polymer's LCST, the PL intensity showed a notable increase and was highest when the temperature was 37 °C. Zhang et al. [42] reported atom transfer radical polymerization techniques through the “arm-first” strategy of core cross-linked multiarm stars made of polyethylene, polystyrene, or polyethylene-*b*-poly( $\epsilon$ -caprolactone) arms and a cross-linked TPE-2St core. As the rigid cross-linked structure of the poly(TPE-2St) core significantly decreased the intramolecular motions of TPE's aromatic ring, the star polymers were highly emissive not only in the aggregate state but also in the dilute solutions.

In this study, one-step reversible addition-fragmentation chain transfer (RAFT) polymerization techniques were employed to obtain a series of TPE-based cross-linked dual stimulus-responsive (i.e., emission and temperature) random diblock copolymers (poly(NIPAm-co-TPE2St)) using the TPE2St monomer as the AIE luminophore and crosslinker. The TPE2St structural effect on the polymer solution's self-assembly and its optical or thermal properties under various temperatures were investigated. Effect of the prepared polymers on the cell viability of the human liver hepatocellular carcinoma cells (HepG2) was studied via the 3-(4,5-dimethylthiazol-2-yl)-2,5-diphenyltetrazolium bromide (MTT) assay. The assay confirmed that the cell viability was over 80% even with high concentrations of TPE2St and a long incubation period. Dynamic light scattering (DLS)

showed that polymer particle size decreased when the temperature was higher than LCST. The polymers showed emission in the HepG2 cells, indicating the cell uptake of the polymers, and cell imaging showed that the particles were located in the cytoplasm. These results indicate that poly(NIPAm-co-TPE2St) is a good candidate for biomedical applications.

## 2. Experimental

### 2.1. Materials

Scheme 1 illustrates the synthesis procedures for the TPE2St monomer. The target intermediate, 4,4'-(1,2-diphenylethene-1,2-diyl)diphenol (TPE2OH, 1), was synthesized following the processes reported previously [42,43]. Scheme 2 illustrates the TPE-based cross-linked PNIPAm with different TPE2St feed molar ratios. The monomer and PNIPAm were prepared following the synthetic routes described in the supplementary information (SI). NIPAm was purified through recrystallization from *n*-hexane twice before use. 2,2'-Azobisisobutyronitrile (AIBN) was recrystallized from ethanol twice. The other reagents were purchased and used without further purification. Reactions were performed with standard Schlenk techniques under nitrogen.

### 2.2. Cell culture and treatments

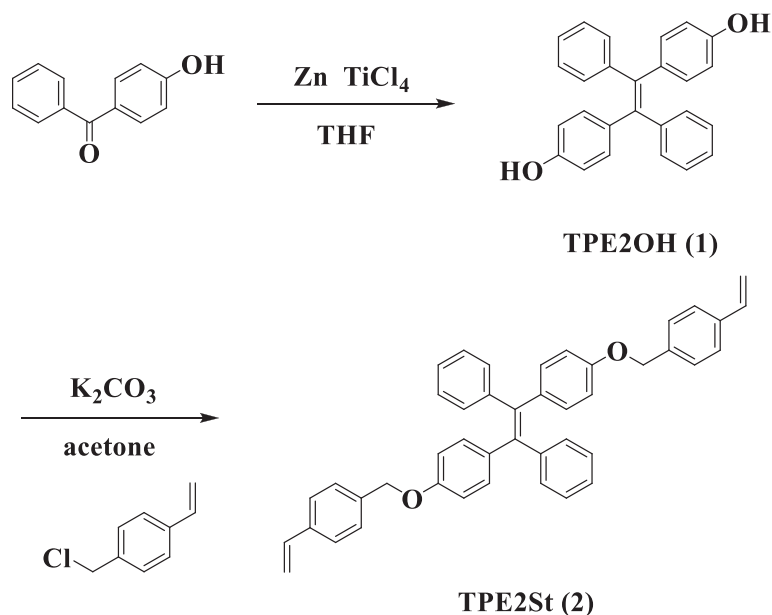
HepG2 and HEK293T cell lines were cultured in Dulbecco's modified Eagle's medium (DMEM, Corning) at 37 °C (in a 5% CO<sub>2</sub> incubator) for 24 h. DMEM was supplemented with 10% (v/v) fetal bovine serum (Biological Industries), L-glutamine, non-essential amino acids, 10 unit/mL penicillin, 10 ng/mL streptomycin, and 25 pg/mL amphotericin B (Biological Industries). The cells were seeded at a density of  $1 \times 10^4$ /well on a 96-well plate. After 24 or 48 h of incubation, the cells were treated with TPE2St-based PNIPAm as the experimental group.

### 2.3. In vitro cell cytotoxicity

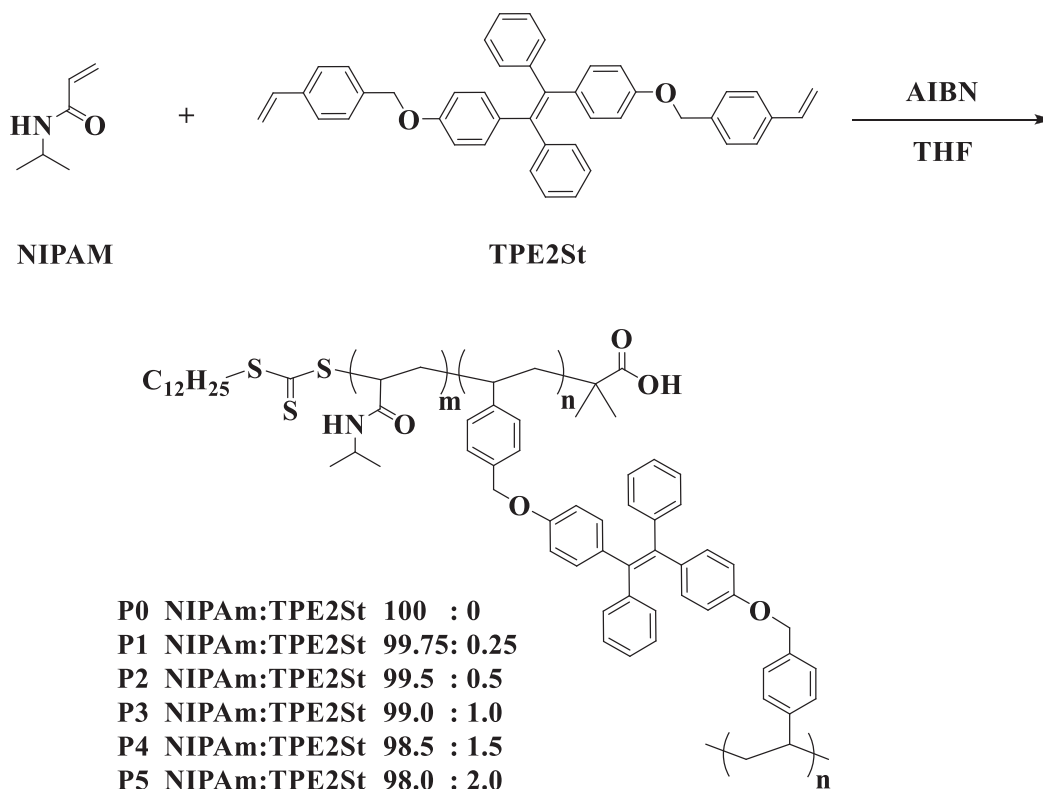
The cell viability was assessed by MTT assay. The MTT solution contained 5 mg/mL thiazolyl blue tetrazolium bromide which was dissolved in phosphate-buffered saline (PBS). Firstly, MTT solution was added into the medium of each well in a 96-well plate. After 2 h of incubation at 37 °C, the culture medium was replaced by dimethyl sulfoxide (DMSO). The cell viability for each well was detected by measuring the optical density at 570 nm in the Hidex Sense microplate reader (Hidex) HEK293T.

### 2.4. Cell imaging

First,  $3 \times 10^5$  HepG2 cells were seeded onto 6-well plates. After 24 h, the medium was replaced with new one with the drug at a concentration of 50  $\mu$ g/mL. After 24 or 48 h, the cells were washed with PBS and treated with 500  $\mu$ L of trypsin-EDTA for 5 min. Then, 2 mL of culture medium was added and the cells were harvested, transferred to 15 mL tubes, centrifuged at 1000 rpm for 5 min. Next, the supernatant was removed, washed with 5 mL of PBS, and centrifuged at 1000 rpm for 5 min. Afterward, the supernatant was removed and the cells were resuspend in 1 mL of PBS. Next, 10  $\mu$ L of PBS was retrieved with the cells, and 10  $\mu$ L of trypan blue was added. A hemacytometer was used to count the cell numbers. The cell suspension was diluted to 100 cells/ $\mu$ L and 100  $\mu$ L of the cell mixture was added to a white 96-well plates (each well had  $1 \times 10^4$  cells). Fluorescence was detected using an ELISA reader, luciferase assay reader, or any instrument that could detect fluorescence. The excitation light wavelength was set at 360 nm and the emission light wavelength was set at 450 or 490 nm. The fluorescent intensities of P2, P3, and P4



**Scheme 1.** Routes to synthesizing the TPE2OH intermediate (1) and TPE2St monomer (2).



**Scheme 2.** Routes to synthesizing the TPE2St-based PNIPAm polymers.

polymers in the cells were measured for 4 days. PL intensity was measured after washing the cells directly (day 0), and after 24 h (day 1), 48 h (day 2), 72 h (day 3), and 96 h (day 4).

### 2.5. Drug loading on P2 and cytotoxicity of the drug loading polymer (DOX-P2)

Doxorubicin hydrochloride (DOX.HCl) was loaded on P2 depending on the hydrophobic forces, which made TPE2St and DOX.HCl aggregate in the aqueous solutions. Drug coating began

with the preparation of the PMs by dissolving 25 mg of P2 in 10 mL of acetone and stirring for 6 h at room temperature. In addition, 5 mg of DOX.HCl was dissolved in 1 mL of DMSO. Then, 2 mL of triethylamine was added to the solution, which was then stirred for 30 min in darkness. The P2 solution was added dropwise to DOX and the mixture was stirred for 24 h in darkness at room temperature. Then, the mixture was dialyzed against DI water for 24 h at room temperature to remove unreacted DOX and organic solvents (dialysis bag MWCO: 1 kD). The final DOX-loaded P2 was stored at -4 °C.

### 3. Results and discussion

#### 3.1. Synthesis of the TPE2St monomer and PNIPAm-containing polymers

The route through which the AIE cross-linker (labeled 2 (TPE2St) in Fig. 1) was prepared and shown in Scheme 1. The TPE intermediate, 4,4'-(1,2-diphenylethene-1,2-diyl)diphenol (1; TPE2OH), at 80 °C were obtained through the McMurry coupling reaction of 4-hydroxybenzophenone in the presence of titanium tetrachloride and zinc. We subsequently prepared 1,2-bis[4-(4-vinylbenzyloxy)phenyl]-1,2-diphenylethene (2; TPE2St) in a 57.2% yield by using a Williamson ether reaction at 100 °C using intermediate 1 and 4-vinylbenzyl chloride as reactants in the presence of potassium carbonate. The <sup>1</sup>H NMR spectrum derived for TPE2St as well as the corresponding proton assignments are displayed in Fig. 1. The presence of the vinyl group doublet of doublets (dd; H<sub>a</sub>, H<sub>b</sub>, and H<sub>c</sub>) in protons at 5.26–6.64 ppm confirmed that the TPE2St was synthesized successfully. Conversely, the shifts δ = 4.99–5.01 and 6.65–7.45 ppm were ascribed to the singlet proton signals of aliphatic methylene (H<sub>d</sub>) and aromatic doublet/triplet proton signals (H<sub>e</sub>, H<sub>f</sub>, H<sub>g</sub>, H<sub>h</sub>, H<sub>i</sub>, and H<sub>j</sub>), respectively.

The RAFT polymerization was performed to synthesize poly(NIPAm-co-TPE2St)s with different feed molar ratios; it was reacted in THF at 60 °C by employing the monomer in a 1000:2:1 [M]<sub>0</sub>: [CTA]<sub>0</sub>: [AIBN]<sub>0</sub> molar ratio. The TPE2St monomer only occupies 0.25–2.0 mol% of the total monomers. The polymerization conditions and results are summarized in Table 1, and Scheme 2 presents the synthetic routes of the poly(NIPAm-co-TPE2St)s. We used <sup>1</sup>H NMR

spectroscopy, recorded in acetone-*d*<sub>6</sub>, to determine the final ratio of NIPAm and TPE2St, which is displayed in Fig. 2 and Table 1. The degree of polymerization (DP) of the poly(NIPAm-co-TPE2St) was calculated based on the integral ratio of methine protons H<sub>b</sub> (3.86–4.12 ppm) derived from the NIPAm monomer, and the aliphatic methylene (H<sub>c</sub>) from the TPE2St, to methyl protons H<sub>a</sub> in the CTA agent (0.86 ppm). We obtained a DP of 192 for homopolymer PNIPAm (P0) and the *M*<sub>n(NMR)</sub> of the polymer was 22.05 kg mole<sup>-1</sup>, according to the following equation:

$$M_{n(NMR)} = (3(H_b/H_a) \times M_{n,NIPAm}) + M_{n,CTA} \quad (1)$$

where *M*<sub>n, NIPAm</sub> and *M*<sub>n, CTA</sub> are the molecular weight of the NIPAm monomer and CTA, respectively, and H<sub>a</sub> and H<sub>b</sub> are the integrals of methyl and methine protons (–CH) protons, respectively. Using GPC, *M*<sub>n</sub> was found to be 18.94 kg mole<sup>-1</sup>. The GPC traces of the synthesized polymers are shown in Fig. S1. Thus, the proportion of NIPAm macro-CTA chains that had their ends capped with CTA groups was roughly equal to 85.9%. From the final ratio of PNIPAm: TPE2St (*m*:*n*), it was found that the ratio of NIPAm decreased by increasing the TPE2St ratio; this can be attributed to the steric hinderance caused by the TPE monomer, as it influenced the RAFT copolymerization, leading to the decrease in NIPAm ratio.

#### 3.2. Thermal and crystalline properties of polymers

TGA was used to analyze the decomposition temperature (*T*<sub>d</sub>) values at 10% weight loss of the polymers, which were in the range of 334.6–359.6 °C. It is notable that the *T*<sub>d</sub> decreased with increase in

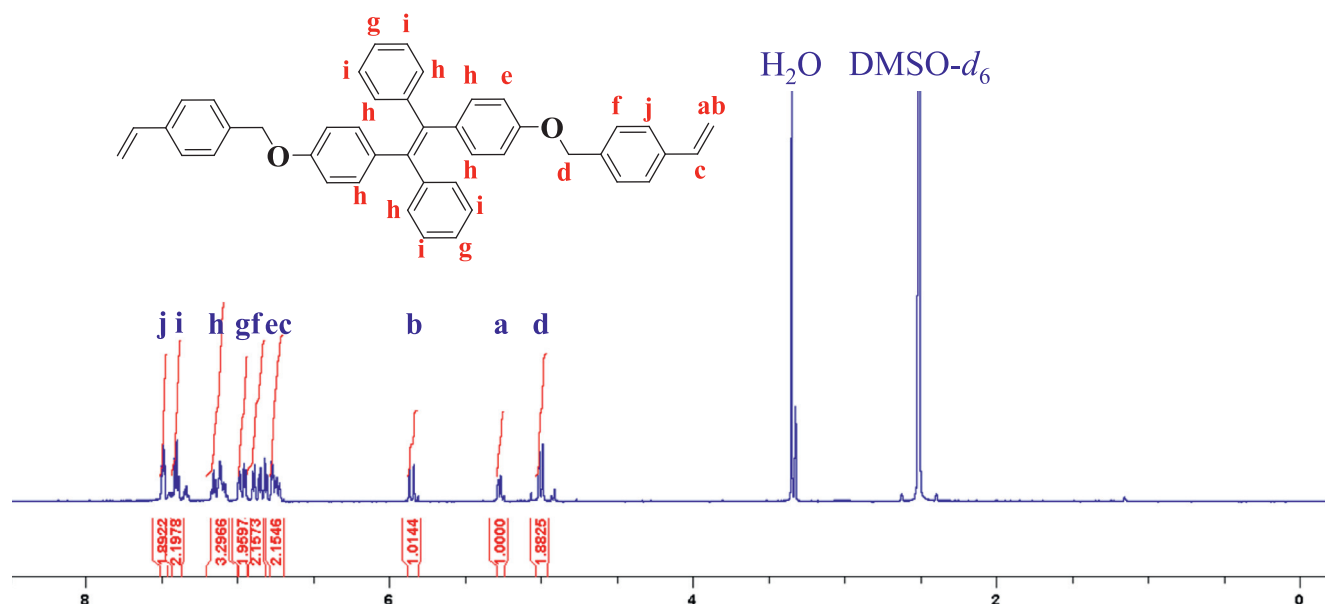


Fig. 1. <sup>1</sup>H NMR spectrum of TPE2St monomer in DMSO-*d*<sub>6</sub>.

Table 1

Molecular weights and thermal properties of polymers.

No	Feed molar ratio NIPAm: TPE2St ( <i>m</i> : <i>n</i> )	Final block length NIPAm: TPE2St ( <i>m</i> : <i>n</i> ) <sup>a</sup>	<i>M</i> <sub>n(NMR)</sub> <sup>a</sup> (kg/mole)	<i>M</i> <sub>n(GPC)</sub> <sup>b</sup> (kg/mole)	PDI <sup>b</sup>	<i>T</i> <sub>g</sub> (°C) <sup>c</sup>	<i>T</i> <sub>d10</sub> (°C) <sup>d</sup>
P0	100:0	192:0	22.05	18.94	1.26	139.0	359.6
P1	99.75:0.25	62.5:0.33	7.61	10.40	1.42	140.9	352.0
P2	99.5:0.5	34.4:0.38	4.39	8.65	1.55	140.4	342.9
P3	99.0:1.0	33.3:0.46	4.57	7.84	1.24	144.0	341.3
P4	98.5:1.5	29.4:0.64	4.16	5.20	1.53	147.0	334.6
P5	98.0:2.0	21.4:0.85	3.56	4.20	1.55	146.8	337.4

<sup>a</sup> Calculated based on the individual integral proton ratio of two monomers using the <sup>1</sup>H NMR spectra.

<sup>b</sup> *M*<sub>n</sub> and PDI of polymer were determined by gel permeation chromatography using polystyrene standards in THF.

<sup>c</sup> Glass transition temperature by DSC under N<sub>2</sub> at a heating rate of 10 °C/min.

<sup>d</sup> The temperatures at 10% weight loss.

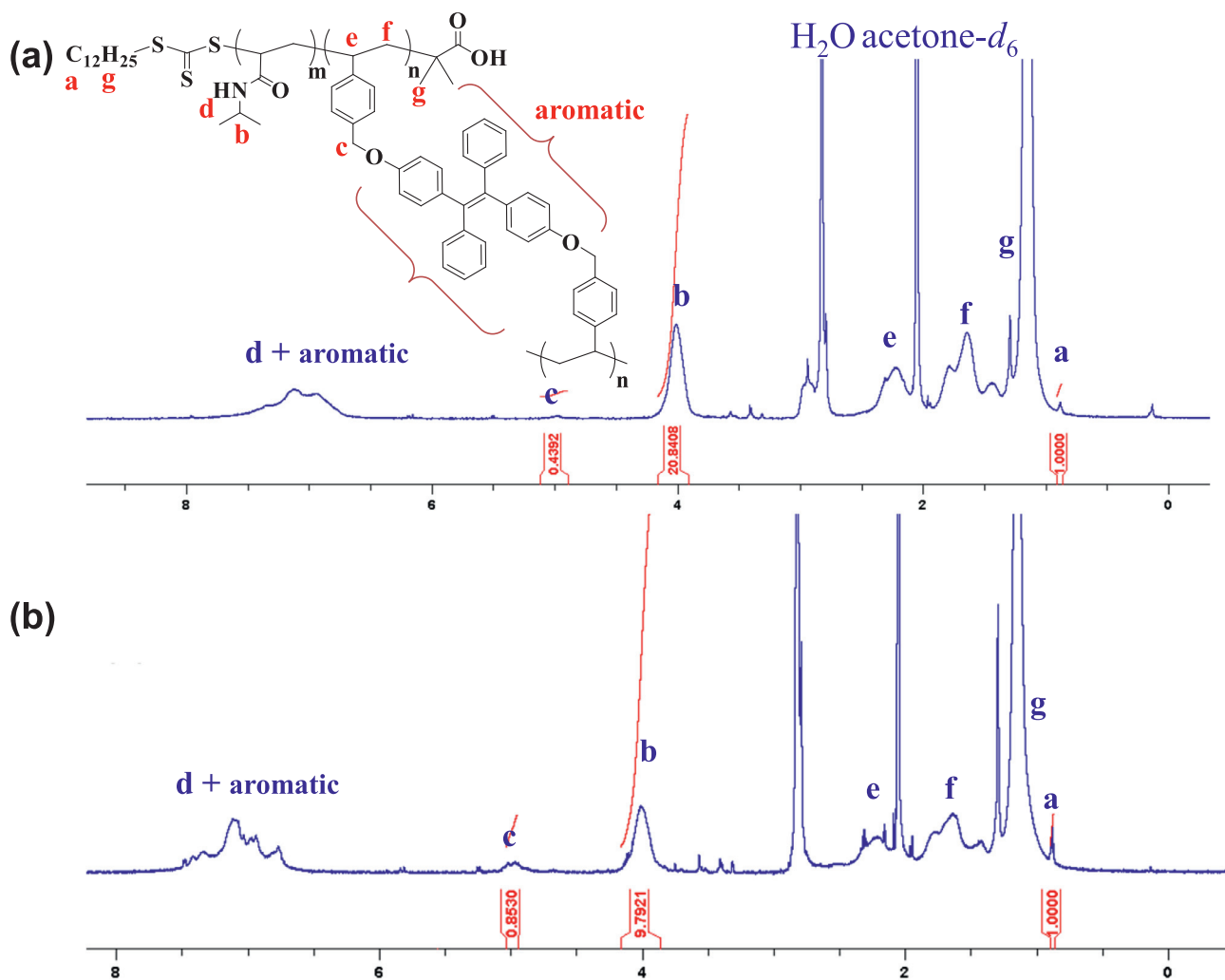


Fig. 2.  $^1\text{H}$  NMR spectra of (a) P1 and (b) P4 in acetone- $d_6$ .

the added amount of TPE2St. This decrease in  $T_d$  can be attributed to the effect of steric hindrances of TPE2St. Polymers with a stronger steric hindrance have high repulsive force and the disturbance caused by heat leads to easier decomposition of these polymers than those with weak steric hindrance [36]. Moreover, the final residual ratio of the polymer at 450–600 °C was relatively higher than that of P0 when the added amount of the TPE2St monomer increased (Fig. S2), revealing that the thermal stability was improved when the bulky TPE segments were incorporated into the copolymer.

The glass transition temperature ( $T_g$ ) of the prepared polymers derived from DSC is summarized in Table 1. It was observed that the  $T_g$  value of the polymers increased as increasing amounts of the cross-linker TPE2St were added. This can be attributed to increases in molecular weight, cross-linking, and the steric hindrance effect; these factors increased when increasing the TPE2St ratio. These results suggest that the  $T_g$  value can be influenced by many factors, e.g., molecular weight, cross-linking density, steric hindrance, bulkiness of the pendants, stiffness of the backbone, symmetry, branching, and polarity [44–46].

XRD of the powder of the prepared polymers (P0, P1, and P2) was carried out to determine the crystallinity properties. The measurements were in the  $2\theta$  range of  $5^\circ$  to  $50^\circ$  with a step size of  $0.05^\circ$ . Fig. S3 shows the XRD pattern of the P0, which exhibited two broad peaks at  $2\theta_1 = 7.83^\circ$  and  $2\theta_2 = 19.98^\circ$  ( $d = 4.44$  Å), indicating an amorphous structure. P1 and P2 also exhibited the same peaks as P0, indicating the governing polymer structure presence of PNIPAm. It is worth

noting that the  $2\theta_2$  values of P1 and P2, i.e.,  $19.87^\circ$  ( $d = 4.46$  Å) and  $19.79^\circ$  ( $d = 4.48$  Å) for P1 and P2, respectively, were smaller than that of P0, implying that the existence of the TPE2St moiety influenced the arrangement of the main P0 structure, leading to the increasing distance between the adjacent side chains.

### 3.3. Thermoresponsive properties of polymers

Thermoresponsive properties of polymers were studied by measuring the LCST and investigating the effect of temperature on the particle size distribution at two different temperatures (e.g.,  $25^\circ\text{C}$  lower than LCST,  $40^\circ\text{C}$  higher than LCST). Generally, PNIPAm in an aqueous solution collapses and forms polymer chain aggregates at approximately  $32^\circ\text{C}$  and the turbidity of the solution increases upon heating to more than  $32^\circ\text{C}$  [47]. Fig. 3 presents the LCST behavior of P0–P5 (2.5 mg/mL). The LCST of P0 was  $32.2^\circ\text{C}$  which is in accordance with the LCST of PNIPAm reported in previous studies [48,49]. By adding TPE2St, it was found that the LCSTs of P1 and P2 ( $33.5^\circ\text{C}$  and  $32.4^\circ\text{C}$ , respectively) were higher than that of P0 ( $32.2^\circ\text{C}$ ). This can be attributed to the repulsion of the PNIPAm chains tethered to the micelle's hydrophobic TPE core [50]. On the other hand, the LCST of P3 decreased to  $28.1^\circ\text{C}$ , indicating that greater amounts of bulky TPE2St destroyed the hydrogen bonds within the PNIPAm chains. Moreover, a large amount of TPE2St monomer increased the hydrophobicity, leading to the decrease of LCST [51,52]. Also, we noted that the phase transition in P4 and P5 was not clear, which can be

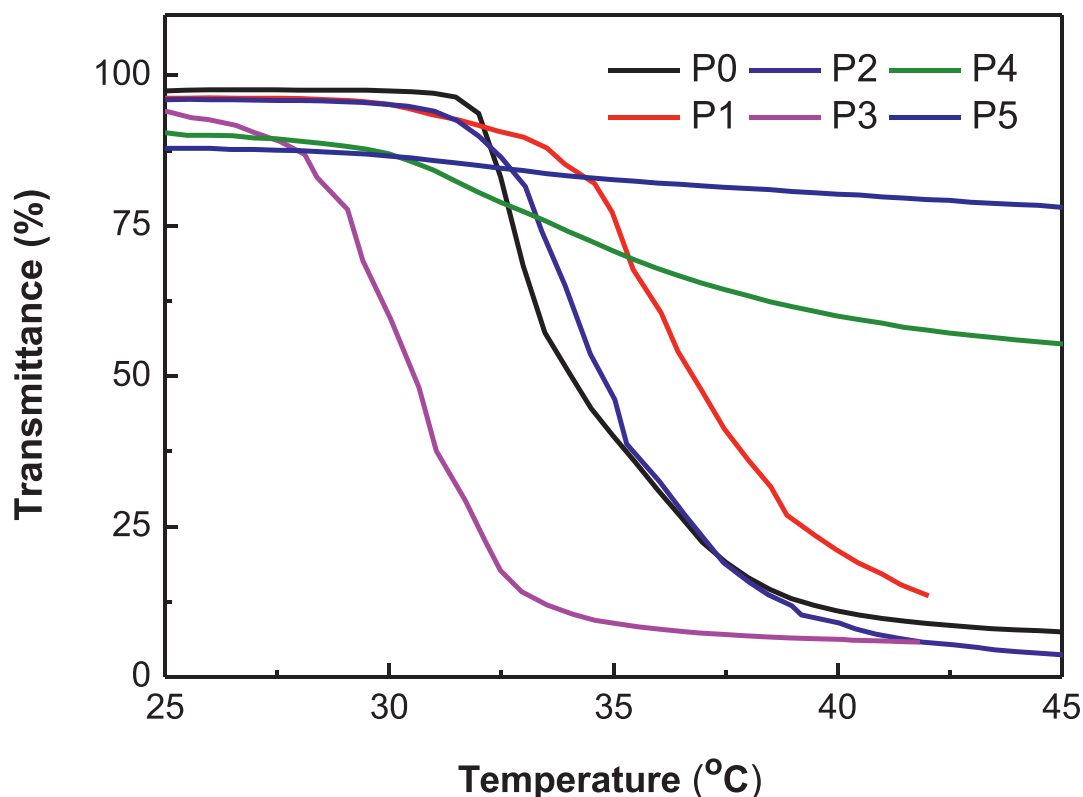


Fig. 3. Thermoresponsive properties of polymers at various temperatures. Concentration of polymers: 2.5 mg/mL in water.

attributed to the higher ratios of TPE2St. Fig. S3 shows the phase transition of the polymer solutions, where lower than LCST polymer solutions were clear (Fig. S4 (a)) and transformed to white or milky solutions when the temperature was higher than the LCST (Fig. S4 (b)).

The effect of temperature on the particle size and size distribution was investigated by DLS measurements. We determined the  $D_h$  of the P0 and P1–P2 nano-assemblies at two temperatures; lower and higher than the LCST (i.e., 25 and 40 °C; Fig. 4). The  $D_h$  of the P0 and P1–P2 at a temperature higher than the LCST decreased from 564.0 to 159.6 nm, 417.4 to 126.7 nm, and 469.4 to 134.5 nm for P0, P1, and P2, respectively. These results indicate that the swollen aggregates of TPE-based cross-linked poly(*N*-isopropylacrylamide)s transformed into separated objects with increasing temperature from 25 to 40 °C. The addition of cross-linker (TPE2St) has been proposed as a means to control the swelling/shrinking ratio of the gels and to add responsiveness toward different stimuli. This can also be attributed to the fact that, above LCST, the coil PNIPAm chains turn to a shrunken state, and a swollen state happens in the transition state. Obviously, above the LCST, shrinking objects formed very stably, and further elevation of temperature to 40 °C led the more aggregated amorphous particles to shrink greatly, and the  $D_h$  reduced to smaller size [53–55]. Regular morphological micelles at 40 °C in an aqueous solution were observed (Fig. 4 (b)). Fig. S5 presents the TEM images of the spherical aggregates obtained using the P0 and P1–P2 (0.5 mg mL<sup>-1</sup>) dissolving in H<sub>2</sub>O. The decreasing phenomenon of  $D_h$  under TEM was consistent with that of DLS.

#### 3.4. Optical properties and AIE effect

UV-vis absorption spectroscopy for the five poly(NIPAm-co-TPE2St)s was recorded in the THF solution ( $1.0 \times 10^{-6}$  M), as shown in Fig. S6. Strong absorption bands were observed in the spectra at 250 nm, which were attributable to the  $\pi-\pi^*$  transition of the polymeric structure. Furthermore, weak absorption bands at

approximately  $315 \pm 15$  nm were engendered by the TPE chromophores. The AIE properties of P1 and P2 (Fig. 5) were investigated in a mixture of THF (solvent)/water (nonsolvent) with a concentration of  $1.0 \times 10^{-5}$  M. Adding water into the THF induces the TPE2St core to aggregate and the PL intensities increased proportionally with the increase of H<sub>2</sub>O fractions added to the THF solution. PL intensity was highest when the water fraction was 90%, and its intensity was enhanced by about 2.2–2.4-fold compared with that of its pure THF solution. Restriction of the intramolecular rotation is the reason for the AIE effect. In dilute THF solutions, intramolecular rotations of the TPE2St molecules are active, thus, the PL intensity is weak. On the other hand, adding H<sub>2</sub>O to the THF solution leads to TPE aggregation and restricts the intramolecular rotation, leading to deactivation of the nonradiative path and activation of radiative decay which enhances the PL intensities [42]. Fig. 5 shows the differences in the emission of the solutions by adding water under UV light. However, the temperature effect on AIE properties of P2 in THF/H<sub>2</sub>O and pure THF under different temperature was shown in Fig. S7. These results indicate that increasing of temperature of P2 solution in the presence of THF/H<sub>2</sub>O of 10/90 vol% led to destroy the restriction of free motion of TPE2St molecules, decreased PL emissions.

#### 3.5. Cell viability

To apply the prepared polymers to biomedical applications, it is important to evaluate the cytotoxicity of the polymers on living cells. Cytotoxicity was measured by the MTT assay in HepG2 and HEK293T cells. The MTT assay was tested for the prepared monomer TPE2St, and polymers (P1–P5) three times to confirm the cell viability at a concentration of 2  $\mu$ g/mL and under further dilutions. The polymers showed cell viability of over 80% after the incubation period reached 24 h (Fig. 6 (a) and Fig. S10 (a)) as well as 48 h (Fig. 6 (b) and Fig. S10 (b)). Herein, the high cell viability that the polymers showed that they were not toxic to living human cancer and non-cancer cell lines.

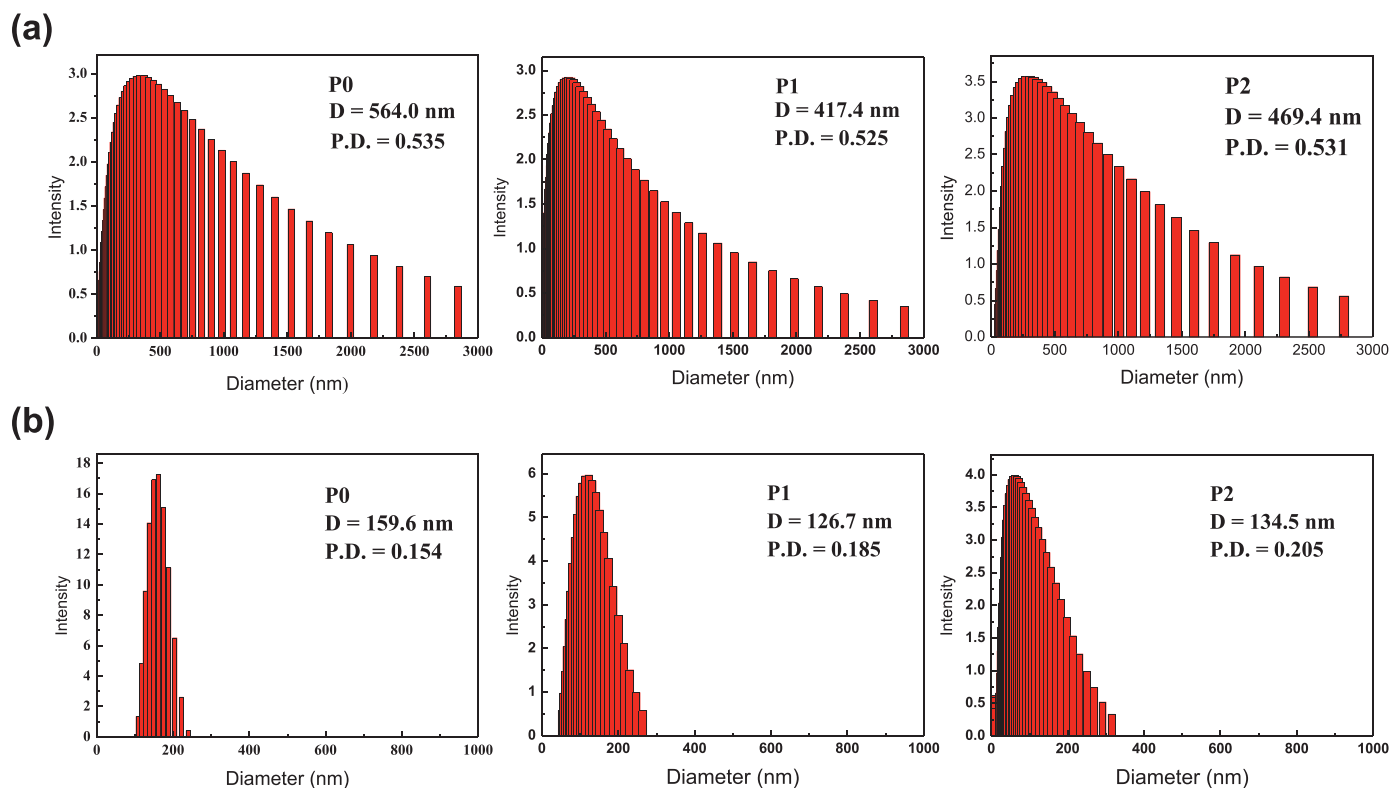


Fig. 4. Particle size distributions of P0 and P1-P2 in water at (a) 25 and (b) 40 °C. (Concentration of 2 mg/10 mL).

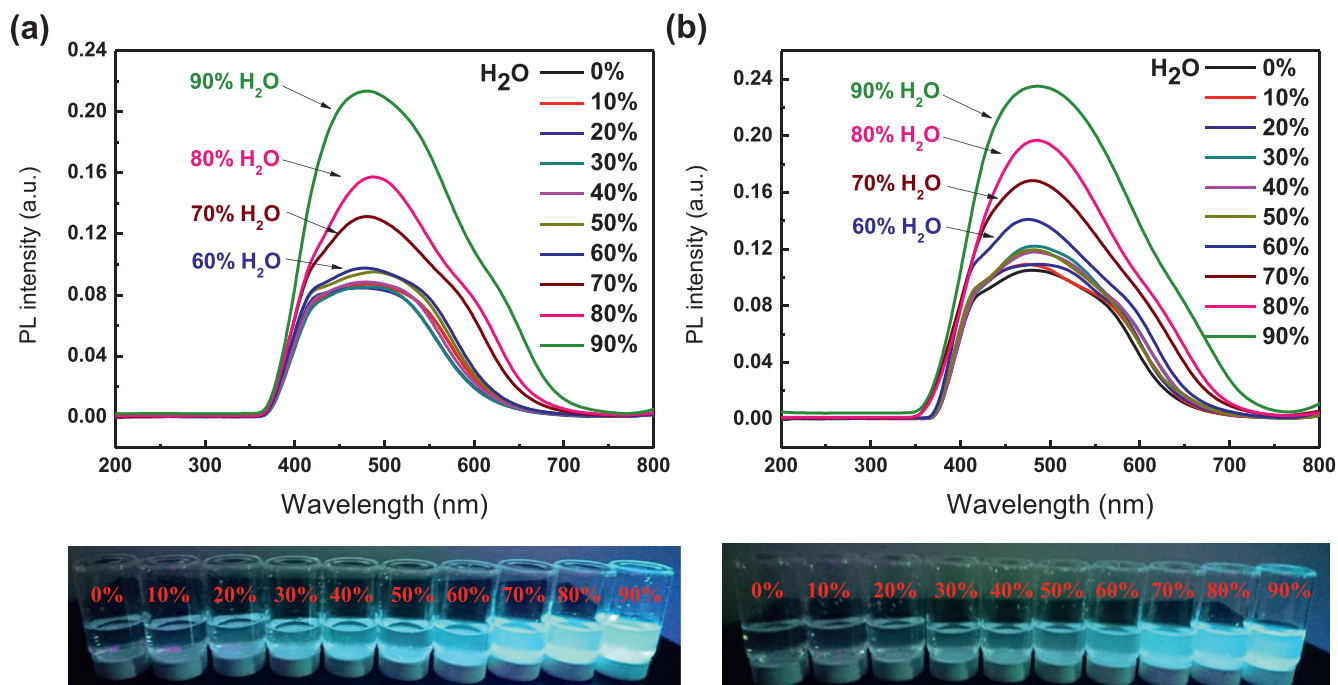


Fig. 5. PL intensity variations of (a) P1 and (d) P2 in the presence of various fractions of THF/H<sub>2</sub>O and their corresponding emission colors under 365 nm UV light at room temperature.

Thus, the prepared polymers could be appropriate carriers and lumiphores for drug delivery and cell imaging in cancer therapy.

### 3.6. Cell imaging

The fluorescence intensity of P1–P3 in HepG2 cancer cells was investigated for 4 days as shown in Fig. 7. It was noticed that the PL

intensity at day 0 was the strongest for the three polymers and decreased with time until it decayed on day 2 for P1 and on day 3 for P2. It did not decay totally for P3 even after the day 4. The amount of TPE2St in each polymer is the reason for the differences in the PL intensities and the long-lived emission, where P3 had a higher ratio of TPE2St than P1 and P2. Thus, it showed the highest and longest PL intensity. It is worth noting that the PL intensity was stronger at an

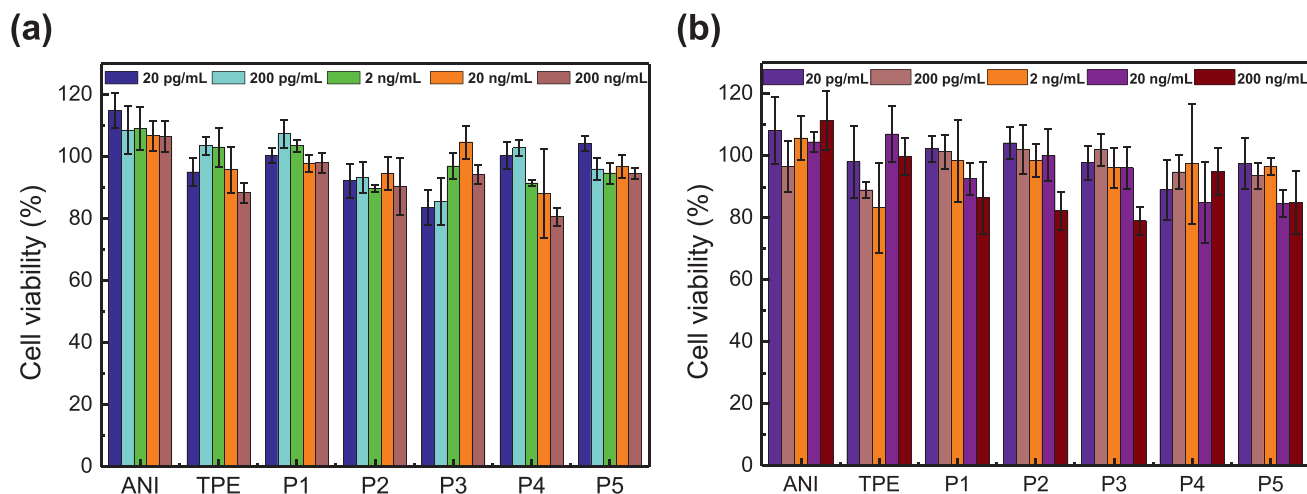


Fig. 6. Percentages of HepG2 cell survival following exposure to various drug concentrations for (a) 24 h and (b) 48 h at 37 °C via MTT cell growth assay.

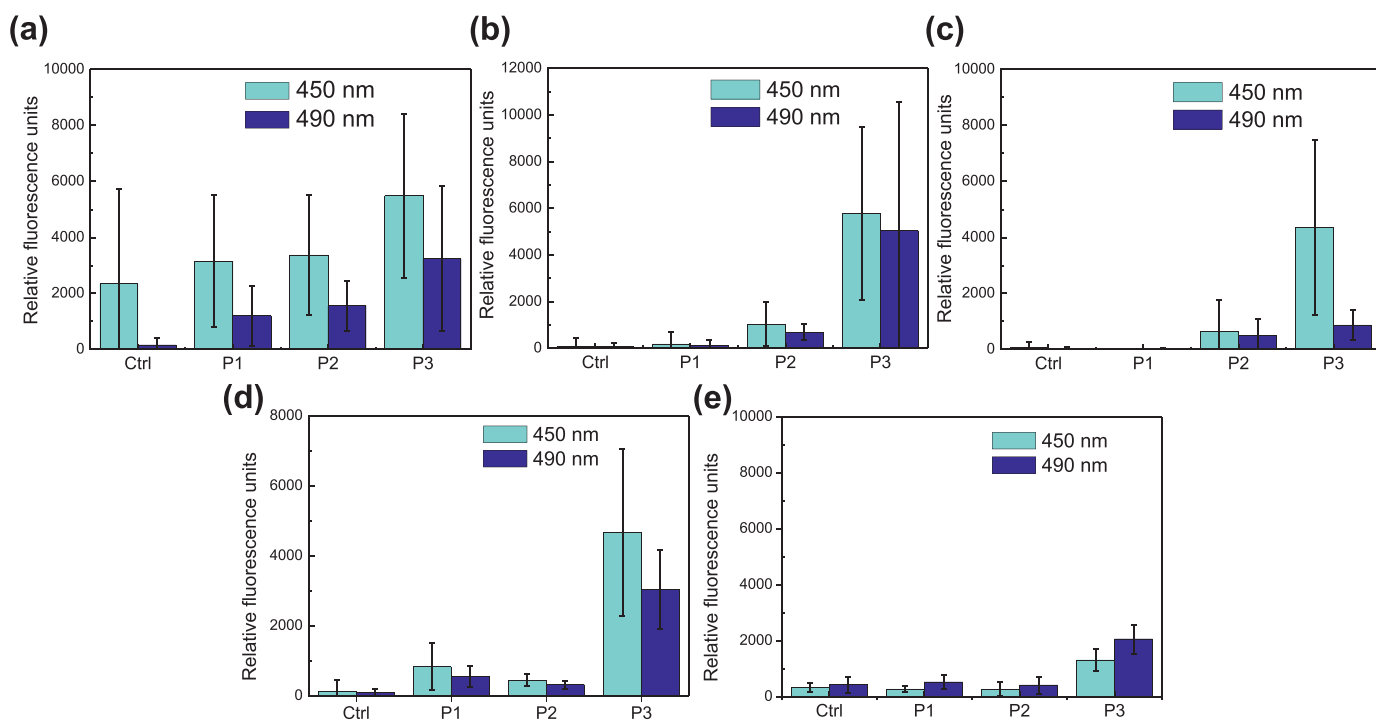


Fig. 7. PL intensity of P1-P3 in HepG2 cancer cells in a concentration of 50 μg/mL after (a) zero time, (b) 24 h, (c) 48 h, (d) 72 h, and (e) 96 h incubation at 37 °C.

emission wavelength of 450 nm than that at 490 nm. Moreover, the decrease of the intensities is a sign that the polymers became soluble and were undergone hydrolysis and cleared [56]. Fig. 8 shows the images of HepG2 cells under fluorescence microscope under daylight and UV light at 360 nm. Images were taken after 24 h of incubation with P1–P3 at a concentration of 50 μg/mL at 37 °C. It was clear that the polymers were located in the cell cytoplasm, which indicated that the cells were able to uptake the polymers. Therefore, the prepared polymers can be used for cell imaging applications.

### 3.7. Drug coating by P2 (Doxorubicin.HCl)

The absorbance of free and P2-coated DOX was measured via UV-vis spectrometer. The absorbance wavelength of free DOX was 485 nm, while that of P2-coated DOX was 503 nm (Fig. S8 (a)). A

redshift occurred because of the hydrogen bonding between the polymer and DOX, as shown in Fig. S8 (b). In addition, the PL intensity of P2-coated DOX was measured at an excitation wavelength of 360 nm; it showed emission peak at a wavelength of 477 nm, which is related to P2. At an excitation wavelength of 490 nm it showed emission at 587 nm, which is related to DOX (Fig. S9). Moreover, the particle size for P2-coated DOX was measured *via* DLS, and it was found that the particle size increased compared to that of P2, as shown in Fig. 9. With these measurements, we can conclude that DOX was successfully loaded onto P2.

## 4. Conclusions

In this study, we prepared five TPE-based cross-linked PNIPAMs through RAFT polymerization and estimated their optical and thermal characteristics. According to the NMR spectra, the RAFT

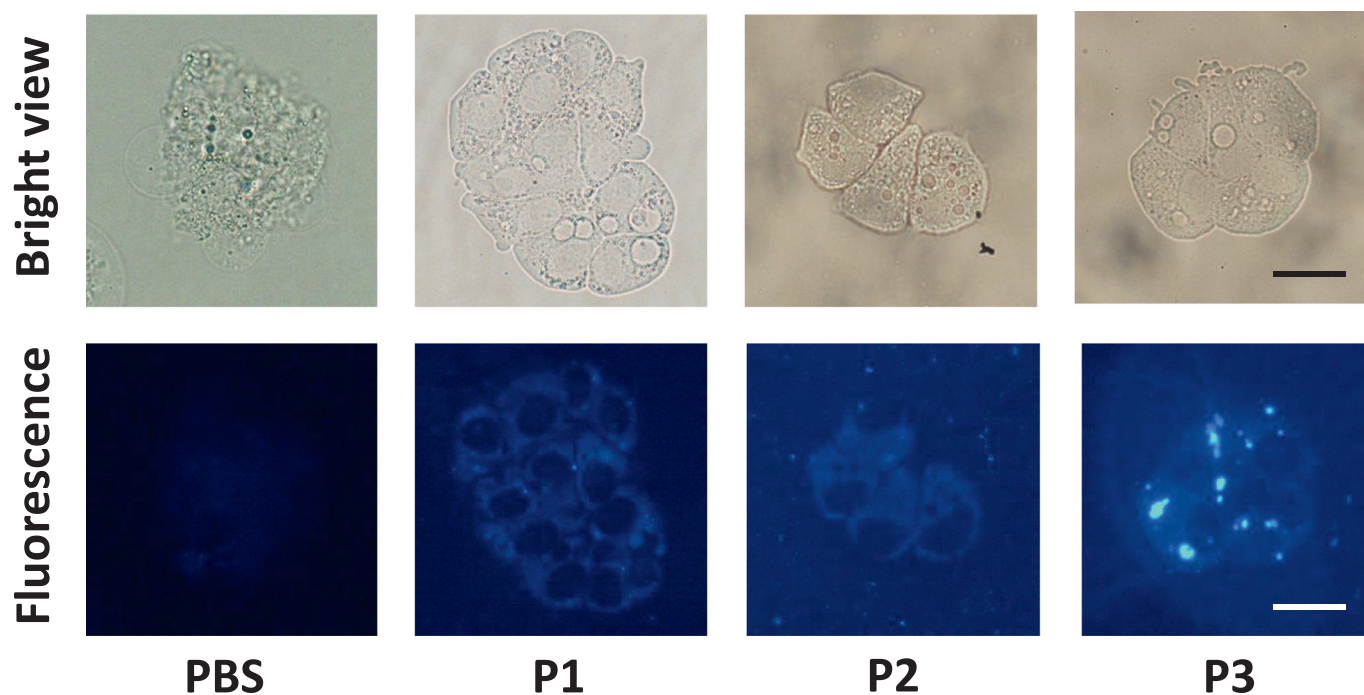


Fig. 8. Images of HepG2 cells under fluorescence microscopy after 24 h incubation with P1-P3 in a concentration of 50  $\mu\text{g}/\text{mL}$  at 37  $^{\circ}\text{C}$ . (Scale bar = 50  $\mu\text{m}$ ).

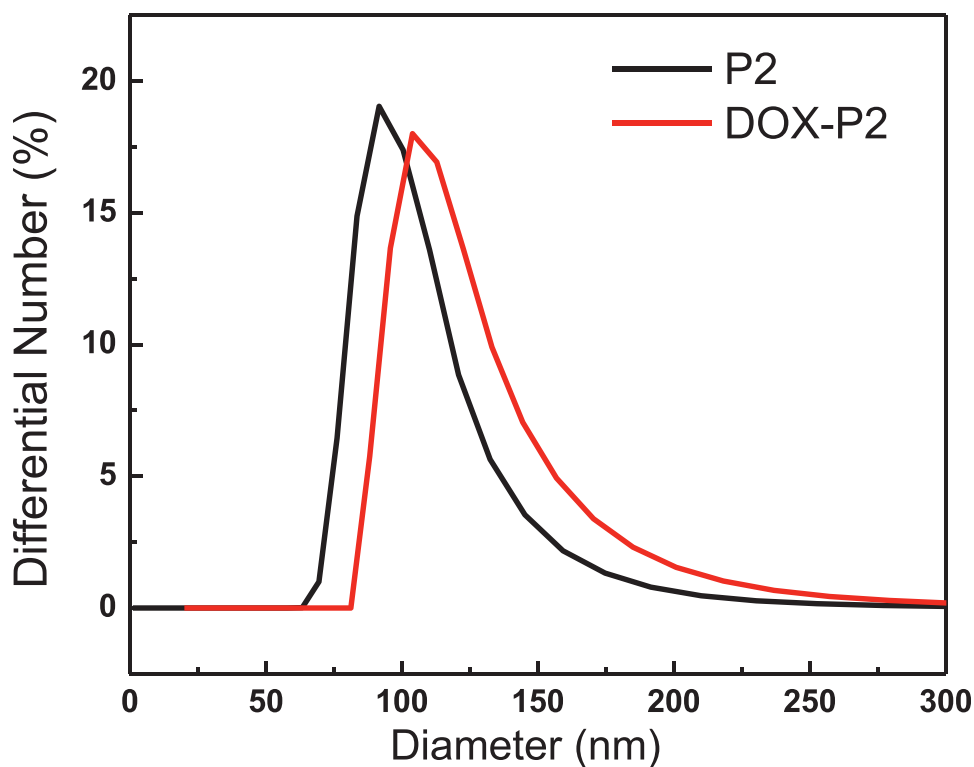


Fig. 9. Particle size distributions of P2 and DOX-P2 in a concentration of 2 mg/10 mL  $\text{H}_2\text{O}$  at 25  $^{\circ}\text{C}$ .

polymerization was successful. XRD patterns confirmed the amorphous structure of the polymers P1 and P2, and TPE2St affected the distance between the polymer side chain molecules. DLS revealed that increasing the temperature in the polymer solution induced microphase separation and the formation of regular micelles. From PL intensity measurements, we confirmed that the prepared polymers showed an AIE effect. The MTT assay of the polymers confirmed that the cell viability was over 80% with high concentrations or a long

incubation period, which means that the polymers are not toxic to living cells.

#### Declaration of Competing Interest

The authors declare that they have no known competing financial interests or personal relationships that could have appeared to influence the work reported in this paper.

## Acknowledgement

This research was supported by the Ministry of Science and Technology, Taiwan (MOSTs 110-2221-E-155-001, 109-2221-E-155-053). The authors thank the staff at National Sun Yat-sen University for assistance with TEM (ID: EM022600) experiments.

## Supplementary materials

Supplementary material associated with this article can be found in the online version at doi:10.1016/j.jtice.2022.104238.

## References

- [1] Gautam A, Chaudhary K, Kumar R, Gupta S, Singh H, Raghava GPS. Managing drug resistance in cancer: role of cancer informatics. *Methods Mol Biol* 2016;1395:299–312.
- [2] Stewart BW, Wild CP. World cancer report 2014. Geneva, Switzerland: International Agency for Research on Cancer, Distributed by WHO Press, World Health Organization; 2014 ISBN 9789283204299.
- [3] Qu C, Chen T, Fan C, Zhan Q, Wang Y, Lu J, Lu LL, Ni Z, Huang F, Yao H, Zhu J, Fan J, Zhu Y, Wu Z, Liu G, Gao W, Zang M, Wang D, Dai M, Hsia CC, Zhang Y. Efficacy of neonatal HBV vaccination on liver cancer and other liver diseases over 30-year follow-up of the qidong hepatitis B intervention study: a cluster randomized controlled trial. *PLoS Med* 2014;11:e1001774.
- [4] Khan NT. Nanoparticles mediated drug delivery. *J Pharmacogenomics Pharmacoproteomics* 2017;8:1000172.
- [5] Xu W, Ling P, Zhang T. Polymeric micelles, a promising drug delivery system to enhance bioavailability of poorly water-soluble drugs. *J Drug Deliv* 2013;2013:15.
- [6] Ahmad Z, Shah A, Siddiq M, Kraatz HB. Polymeric micelles as drug delivery vehicles. *RSC Adv* 2014;4:17028–38.
- [7] Zhou Q, Zhang L, Yang TH, Wu H. Stimuli-responsive polymeric micelles for drug delivery and cancer therapy. *Int J Nanomedicine* 2018;13:2921–42.
- [8] Bagheri M, Fens MH, Kleijn TG, Capomaccio RB, Mehn D, Krawczyk PM, Scutigliani EM, Gurinov A, Baldus M, Kronenburg NCH, Kok RJ, Heger M, van Nostrum CF, Hennink WE. *In vitro* and *in vivo* studies on HPMA-based polymeric micelles loaded with curcumin. *Mol Pharma* 2021;18:1247–63.
- [9] Wang Z, Yong TY, Wan J, Li ZH, Zhao H, Zhao Y, Gan L, Yang XL, Xu HB, Zhang C. Temperature-sensitive fluorescent organic nanoparticles with aggregation-induced emission for long-term cellular tracing. *ACS Appl Mater Interfaces* 2015;7:3420–5.
- [10] Zhou H, Liu F, Wang X, Yan H, Song J, Ye Q, Tang BZ, Xu J. Aggregation induced emission based fluorescence pH and temperature sensors: probing polymer interactions in poly(*N*-isopropyl acrylamide-co-tetra(phenyl)ethene acrylate)/poly(methacrylic acid) interpenetrating polymer networks. *J Mater Chem C* 2015;3:5490–8.
- [11] Li T, He S, Qu J, Wu H, Wu S, Zhao Z, Qin A, Hu R, Tang BZ. Thermoresponsive AIE polymers with fine-tuned response temperature. *J Mater Chem C* 2016;4:2964–70.
- [12] Ma H, Qi C, Cheng C, Yang Z, Cao H, Yang Z, Tong J, Yao X, Lei Z. AIE-active tetraphenylethylene cross-linked *N*-isopropylacrylamide polymer: a long-term fluorescent cellular tracker. *ACS Appl Mater Interfaces* 2016;8:8341–8.
- [13] Yang PC, Chien YH, Tseng SH, Lin CC, Huang KY. Synthesis and self-assembly of multistimulus-responsive azobenzene-containing diblock copolymer through RAFT polymerization. *Polymers* 2019;11:2028.
- [14] Schild HG. Poly(*N*-isopropylacrylamide): experiment, theory and application. *Prog Polym Sci* 1992;17:163–249.
- [15] Lai EP, Wang YX, Wei Y, Li G. Preparation of uniform-sized and dual stimuli-responsive microspheres of poly(*N*-isopropylacrylamide)/poly(acrylic acid) with semi-IPN structure by one-step method. *Polymers* 2016;8:90.
- [16] Tauer K, Gau D, Schulze S, Völkel A, Dimova R. Thermal property changes of poly(*N*-isopropylacrylamide) microgel particles and block copolymers. *Colloid Polym Sci* 2009;287:299–312.
- [17] Kocardekar RR, Shah VK, Mody H. PNIPAm poly(*N*-isopropylacrylamide): a thermoresponsive “smart” polymer in novel drug delivery systems. *IJMU* 2012;7:59–62.
- [18] Durme KV, Rahier H, Mele BV. Influence of additives on the thermoresponsive behavior of polymers in aqueous solution. *Macromolecules* 2005;38:10155–63.
- [19] Duan Q, Narumi A, Miura Y, Shen X, Sato SI, Satoh T, Kakuchi T. Thermoresponsive property controlled by end-functionalization of poly(*N*-isopropylacrylamide) with phenyl, biphenyl, and triphenyl groups. *Polym J* 2006;38:306–10.
- [20] Kim SH, Hwang IJ, Gwon SY, Son YA. Photoregulated optical switching of poly(*N*-isopropylacrylamide) hydrogel in aqueous solution with covalently attached spironaphthoxazine and *D*- $\pi$ -A type pyran-based fluorescent dye. *Dyes Pigments* 2010;87:158–63.
- [21] Mei J, Leung NLC, Kwok RTK, Lam JWY, Tang BZ. Aggregation-induced emission: together we shine, united we soar!. *Chem Rev* 2015;115:11718–940.
- [22] Luo J, Xie Z, Xie Z, Lam JWY, Cheng L, Chen H, Qiu C, Kwok HS, Zhan X, Liu Y. Aggregation-induced emission of 1-methyl-1,2,3,4,5-pentaphenylsilole. *Chem Commun* 2001;18:1740–1.
- [23] Chen Y, Lam JWY, Kwok RTK, Liu B, Tang BZ. Aggregation-induced emission: fundamental understanding and future developments. *Mater Horiz* 2019;6:428–33.
- [24] Morishima K, Ishiwari F, Matsumura S, Fukushima T, Shibayama M. Mesoscopic structural aspects of Ca<sup>2+</sup>-triggered polymer chain folding of a tetraphenylethene-appended poly(acrylic acid) in relation to its aggregation-induced emission behavior. *Macromolecules* 2017;50:5940–5.
- [25] Mohamed MG, Chen TC, Kuo SW. Solid-state chemical transformations to enhance gas capture in benzoxazine-linked conjugated microporous polymers. *Macromolecules* 2021;54:5866–77.
- [26] Samy MS, Mohamed MG, El-Mahdy AFM, Mansoure TH, Wu KCW, Kuo SW. High-performance supercapacitor electrodes prepared from dispersions of tetrabenzonaphthalene-based conjugated microporous polymers and carbon nanotubes. *ACS Appl Mater Interfaces* 2021;13:51906–16.
- [27] Mohamed MG, Tsai MY, Wang CF, Huang CF, Danko M, Dai L, Chen T, Kuo SW. Multifunctional polyhedral oligomeric silsesquioxane (POSS) based hybrid porous materials for CO<sub>2</sub> uptake and iodine adsorption. *Polymers* 2021;13:221.
- [28] Mohamed MG, Ahmed MMM, Du WY, Kuo SW. Meso/microporous carbons from conjugated hyper-crosslinked polymers based on tetraphenylethene for high-performance CO<sub>2</sub> capture and supercapacitor. *Molecules* 2021;26:738.
- [29] Samy MM, Mohamed MG, Kuo SW. Pyrene-functionalized tetraphenylethylene polybenzoxazine for dispersing single-walled carbon nanotubes and energy storage. *Compos Sci Technol* 2020;199:108360.
- [30] Mohamed MG, El-Mahdy AFM, Meng TS, Samy MM, Kuo SW. Multifunctional hypercrosslinked porous organic polymers based on tetraphenylethene and triphenylamine derivatives for high-performance dye adsorption and supercapacitor. *Polymers* 2020;12:2426.
- [31] Zhang X, Mohamed MG, Xin Z, Kuo SW. A tetraphenylethylene-functionalized benzoxazine and copper(II) acetylacetonate form a high-performance polybenzoxazine. *Polymer* 2020;201:122552.
- [32] Mohamed MG, Atayde EC, Matsagar BM, Na J, Yamauchi Y, Wu KCW, Kuo SW. Construction hierarchically mesoporous/microporous materials based on block copolymer and covalent organic framework. *J Taiwan Inst Chem Eng* 2020;122:180–92.
- [33] Tang BZ, Zhan X, Yu G, Pui P, Lee S, Liu Y, Zhu D. Efficient blue emission from siloles. *J Mater Chem* 2001;11:2974–8.
- [34] Tong H, Dong Y, Hong Y, Haussier M, Lam JWY, Sung HHY, Yu X, Sun J, Williams ID, Kwok HS. Aggregation-induced emission: effects of molecular structure, solid-state conformation, and morphological packing arrangement on light-emitting behaviors of diphenyldibenzofulvene derivatives. *J Phys Chem C* 2007;111:2287–94.
- [35] Mei J, Hong Y, Lam JWY, Qin A, Tang Y, Tang BZ. Aggregation-induced emission: The whole is more brilliant than the parts. *Adv Mater* 2014;26:5429–79.
- [36] Pucci A. Mechanochromic fluorescent polymers with aggregation-induced emission features. *Sensors* 2019;19:4969.
- [37] Wu J, Liu W, Ge J, Zhang H, Wang P. New sensing mechanisms for design of fluorescent chemosensors emerging in recent years. *Chem Soc Rev* 2011;40:3483–95.
- [38] Hong Y, Lam JWY, Tang BZ. Aggregation-induced emission. *Chem Soc Rev* 2011;40:5361–88.
- [39] Qin A, Lam JWY, Tang BZ. Luminogenic polymers with aggregation-induced emission characteristics. *Prog Polym Sci* 2010;37:182–209.
- [40] Su Y, Shi W, Chen X, Zhao S, Hui Y, Xie Z. An aggregation-induced emission enhancement fluorescent benzoxazine-derived macromolecule: catalyst-free synthesis and its preliminary application for the determination of aqueous picric acid. *RSC Adv* 2016;6:41340–7.
- [41] Li M, Song X, Zhang T, Zeng L, Xing J. Aggregation induced emission controlled by a temperature-sensitive organic-inorganic hybrid polymer with a particular LCST. *RSC Adv* 2016;6:86012–8.
- [42] Zhang Z, Bilalis P, Zhang H, Gnanou Y, Hadjichristidis N. Core cross-linked multi-arm star polymers with aggregation-induced emission and temperature responsive fluorescence characteristics. *Macromolecules* 2017;50:4217–26.
- [43] Zhang Z, Hadjichristidis N. Temperature and pH-dual responsive AIE-Active core crosslinked polyethylene-poly(methacrylic acid) multimiktoarm star copolymers. *ACS Macro Lett* 2018;7:886–91.
- [44] Liao J, Liu S, Yuan Y, Zhang H. Steric hindrance effect on the thermo- and photo-responsive properties of pyrene-based polymers. *New J Chem* 2018;42:5698–708.
- [45] Gargallo L, Russo M. Effect of structure on glass transition temperatures of poly(methacrylic ester)s with bulky side groups. *Die Makromol Chem* 1975;176:2735–44.
- [46] Xie R, Weisen AR, Lee Y, Aplan MA, Fenton AM, Masucci AE, Kempe F, Sommer M, Pester CW, Colby RH. Glass transition temperature from the chemical structure of conjugated polymers. *Nat Commun* 2020;11:1–8.
- [47] Sahn M, Yildirim T, Dirauf M, Weber C, Sungur P, Hoepfner S, Schubert US. LCST behavior of symmetrical PNIPAm-*b*-P(EO-*b*-PNIPAm) triblock copolymers. *Macromolecules* 2016;49:7257–67.
- [48] Halperin A, Kröger M, Winnik FM. Poly(*N*-isopropylacrylamide) phase diagrams: fifty years of research. *Angew Chem Int Ed* 2015;54:15342–67.
- [49] Rimmer S, Soutar I, Swanson L. Switching the conformational behaviour of poly(*N*-isopropyl acrylamide). *Polym Int* 2009;58:273–8.
- [50] Hemraz UD, Lu A, Sunasee R, Boluk Y. Structure of poly(*N*-isopropylacrylamide) brushes and steric stability of their grafted cellulose nanocrystal dispersions. *J Colloid Interface Sci* 2014;430:157–65.
- [51] García-Peñas A, Biswas CS, Liang W, Wang Y, Yang P, Stadler FJ. Effect of hydrophobic interactions on lower critical solution temperature for poly(*N*-isopropylacrylamide-co-dopamine methacrylamide) copolymers. *Polymers* 2019;11:991.
- [52] Vatankhah-Varnoosfaderani M, Hashmi S, Ghavaminejad A, Stadler FJ. Rapid self-healing and triple stimuli responsiveness of a supramolecular polymer gel based

- on boron-catechol interactions in a novel water-soluble mussel-inspired copolymer. *Polym Chem* 2014;5:512–3.
- [53] Gihm SH, An BK, Chung J, Park CR, Kwon SK, Park SY. Color-tuned highly fluorescent organic nanowires/nanofabrics: Easy massive fabrication and molecular structural origin. *J Am Chem Soc* 2009;131:3950–7.
- [54] Ma H, Ma Y, Li W, Wang F, Zhu F, Qi C, Zhang Z, Yao X, Lei Z. Triphenylamine-based fluorescent soft matter: Interlaced methyl cinnamate groups as the dominant interaction tools for gel formation. *Macromol Chem Phys* 2014;215:2305–10.
- [55] Ma H, Qi C, Cheng C, Yang Z, Cao H, Yang Z, Tong J, Yao X, Lei Z. AIE-active tetraphenylethylene cross-linked *N*-isopropylacrylamide polymer: a long-term fluorescent cellular tracker. *ACS Appl Mater Interfaces* 2016;8:8341–8.
- [56] Cui Z, Lee BH, Pauken C, Vernon BL. Degradation, cytotoxicity and biocompatibility of NIPAAm-based thermosensitive, injectable and bioresorbable polymer hydrogels. *J Biomed Mater Res A* 2011;98(2):159–66.